Valence-band structure and critical point energies of diamond along [100]

M. T. Edmonds,[1,*] A. Tadich,[1,2] M. Wanke,[1,3] K. M. O'Donnell,[2] Y. Smets,[1] K. J. Rietwyk,[1]
J. D. Riley,[1] C. I. Pakes,[1] and L. Ley[1,4]

[1]*Department of Physics, La Trobe University, Bundoora, Victoria 3086, Australia*
[2]*Australian Synchrotron, 800 Blackburn Road, Clayton, Victoria 3168, Australia*
[3]*Institut für Physik, Technische Universität Chemnitz, Reichenhainer Str. 70, 01926 Chemnitz, Germany*
[4]*Institut für Technische Physik, Universität Erlangen, Erwin-Rommel Str. 1, 91058 Erlangen, Germany*

(Received 8 November 2012; published 19 February 2013)

Accurate valence-band dispersions $E(k_\perp)$ have been determined for the technologically relevant Γ-Δ-X symmetry direction of hydrogen-terminated diamond (100) using normal emission angle-resolved photoemission spectroscopy for photon energies between 30 and 206 eV. By analyzing the data using a free-electron final-state model, the emission features can be well understood by assuming primary cone transitions. Critical point energies in the valence band are in good agreement with self-consistent quasiparticle GW calculations. Substantial modulations in the valence-band dispersion occurring in specific regions of the Brillouin zone have been traced to band crossings in the unoccupied free-electron final state. A one-band effective mass of $(0.39 \pm 0.30)m_0$ is determined from the band dispersion close to the Γ point and compared with values in the literature.

DOI: 10.1103/PhysRevB.87.085123 PACS number(s): 71.20.Mq, 81.05.ug, 79.60.Bm

I. INTRODUCTION

Diamond, over the last twenty years, has been investigated as a possible alternative to conventional group IV and III-V semiconductors in a wide range of electronic applications. These include field-effect transistors (FETs) for high-power high-frequency electronic devices,[1,2] solution gated FETs for biological and chemical sensing applications,[3–6] and thermionic and field emitters, which rely on the negative electron affinity of hydrogenated diamond.[7] Recently, diamond has also shown considerable potential in the field of quantum computing applications by utilizing the spin states of diamond defects.[8]

Despite these efforts, experimental knowledge of the electronic band structure of diamond is relatively poor in comparison to other group IV and III-V semiconductors such as Si, Ge, and GaAs. This may largely be attributed to the difficulty in obtaining atomically flat, high-quality, doped single-crystal diamonds as they are needed for angle-resolved photoemission (ARPES), for example. This fact is highlighted by numerous theoretical band structures reported in the literature utilizing density-functional theory (DFT), $\mathbf{k}\cdot\mathbf{p}$, and GW calculations[9–14] compared with a relatively small body of experimental work that has mainly focused on the band structure of diamond along [111].[15–17] The only band mapping performed on (100) diamond surfaces was focused on the surface state dispersion $E(k_\parallel)$ of hydrogen-terminated and bare diamonds in the (100) plane and has not considered the bulk valence-band dispersion along the surface normal.[18–21] Furthermore, even basic parameters such as the carrier effective masses have yet to be reliably determined experimentally.[22] Given the technological relevance of the (100) surface for device applications, an experimentally determined band structure along [100] is of fundamental importance and is now well overdue since the sample problem has been resolved in recent years through the availability of high-quality synthetic diamond that can be polished to sub-nano-meter surface roughness using different types of plasma etching.[23,24]

In the present work, the surface and bulk band structure and critical point energies of both the valence and conduction bands along the [100] direction are determined utilizing angle-resolved photoemission spectroscopy (ARPES), performed at normal emission, on a hydrogen-terminated (100) diamond surface. By densely stepping the excitation energy, the valence-band dispersion $E(k_\perp)$ is mapped out in detail using a free-electron final-state model (FEFS) to determine $k_\perp$, the component of the electron wave vector perpendicular to the surface. The experimental dispersion is compared to DFT and GW band-structure calculations. Critical point energies in the valence band are shown to be in quite good agreement with self-consistent quasiparticle GW calculations. Modulations in the valence-band dispersion at certain regions in the Brillouin zone are a direct result of band crossing points in the free-electron final state where degeneracies are lifted in the real band structure and final-state gaps are opened. A one-band effective mass is determined from the band dispersion in the immediate vicinity of Γ and compared with theoretical predictions and previously reported experimental values.

II. EXPERIMENTAL DETAILS

A synthetic boron-doped single-crystal sample with [100] surface normal with a boron concentration of 5×10^{18} to 5×10^{19} cm^{-3} was used in this study.[25] The sample was cleaned and hydrogen-terminated using the techniques described by Riedel *et al.*[26] The sample was then exposed to air before being transferred to ultrahigh vacuum where it was subsequently annealed to 550 °C for 1 hour to remove airborne hydrocarbon contamination and any air-induced surface conductivity without impairing the hydrogen termination. At this stage, low-energy electron diffraction (LEED) measurements are representative of a well ordered two-domain (2×1)-reconstructed surface. The ARPES measurements were carried out at room temperature and were performed using the La Trobe University toroidal electron analyzer at BESSY II. To measure the band structure along the Γ-Δ-X direction,

measurements were performed in a normal emission geometry, using finely stepped photon energies between 30 and 206 eV, with a total energy and angular resolution of better than 150 meV and 0.2° for $h\nu < 100$ eV, respectively.[27] The energy resolution was approximately 300 meV at $h\nu = 206$ eV, the highest photon energy used in this study. At each photon energy, the Fermi energy E_F was determined using a gold foil reference in Ohmic contact with the diamond sample. All binding energies are referenced to E_F.

Theoretical band structures were calculated using a two-atom basis cell, and a $6 \times 6 \times 6$ Monkhurst-Pack k-point grid. Density functional calculations were performed using the Elk all-electron FP-LAPW code[28] and a Tran-Blaha meta-generalized gradient approximation (MGGA) functional.[29] GW calculations were performed using the ABINIT code within the projector-augmented wave scheme.[30] Numerical integration via contour deformation[31] was used instead of a plasmon-pole model to avoid difficulties deep in the valence band. A plane wave cutoff energy of 16 Hartree was used throughout, with a fine plane wave cutoff of 40 Hartree used for the GW exchange portion of the calculation and a 24 Hartree cutoff for the calculation of the inverse dielectric function. The screening and self-energy portions of the GW calculation were treated on a $10 \times 10 \times 10$ Γ-centered regular grid of k points with 208 bands per k point. G_0W_0 (non-self-consistent) corrections were then calculated for six points along the Γ-X axis for each band, with the corrections then linearly interpolated to the finer Γ-X bands generated using a conventional GGA DFT calculation with the Perdue-Burke-Ernzerhof functional.[32] The resulting MGGA and G_0W_0 band structures have an indirect band gap of 4.38 and 5.6 eV, respectively. All conduction band energies for the MGGA band structure were then corrected using the "scissors" method to agree with the experimentally determined indirect band gap of 5.47 eV.

III. RESULTS AND DISCUSSION

Band structure mapping of a three-dimensional material such as diamond with a crystallographically well-ordered surface relies on the traditional three step model of photoemission with direct, i.e., **k**-conserving optical transitions in the bulk and an escape of the excited photoelectron into vacuum under conservation of the component of its **k** vector parallel to the surface. For normal emission, $\vec{k}_{\text{IIOutside}} = \vec{k}_{\text{II}f} = \vec{k}_{\text{II}i} = 0$ and hence the band structure $E_i(\vec{k}_{\perp i}, \vec{k}_{\text{II}i} = 0)$ follows from energy conservation ($E_{\text{kin}} = E_f = E_i + h\nu$) and the assumption of direct optical transitions between initial states $E_i(\vec{k}_{\perp i}, \vec{k}_{\text{II}i} = 0)$ and free-electron-like final states $E_f(\vec{k}_{\perp f}, \vec{k}_{\text{II}f} = 0)$. The difference between the kinetic energy as measured, E_{kin}, and the final-state energy inside the solid, E_f, amounts to the so-called inner potential V_0. Hence we have

$$\vec{k}_{\perp i} = \vec{k}_{\perp f} = \left[\frac{2m}{\hbar^2}(E_{\text{kin}} - V_0)\right]^{1/2} \quad (1)$$

for the component of $k_\perp$ of both initial and final state of an interband transition that gives rise to a peak in the energy distribution curve (EDC) at an energy E_{kin}. The free-electron final-state (FEFS) model has been used successfully in the past to map the band structures of group IV and III-V semiconductors such as germanium, silicon, and GaAs.[33–36]

All **k** vectors in this work will be presented in the reduced zone scheme, where the true initial state wave vector is obtained by mapping back the final-state wave vector via an appropriate reciprocal lattice vector $\vec{k}_{\perp i} = \vec{k}_{\perp f} - \vec{G}$, where $\vec{G}$ is a bulk reciprocal lattice vector. The Brillouin zone dimension of diamond along [100] is Γ-Δ-$X = 2\pi/a = 1.762$ Å^{-1}.

Figure 1 shows normal emission EDCs obtained as a function of photon energy for (a) $h\nu = 30-80$ eV with a step size of 1 eV between 30–64 eV (excluding the EDC at 37 eV) and 2 eV between 64–80 eV. (b) $h\nu = 82-136$ eV with a step size of 2 eV between 82–112 eV and 10 eV between

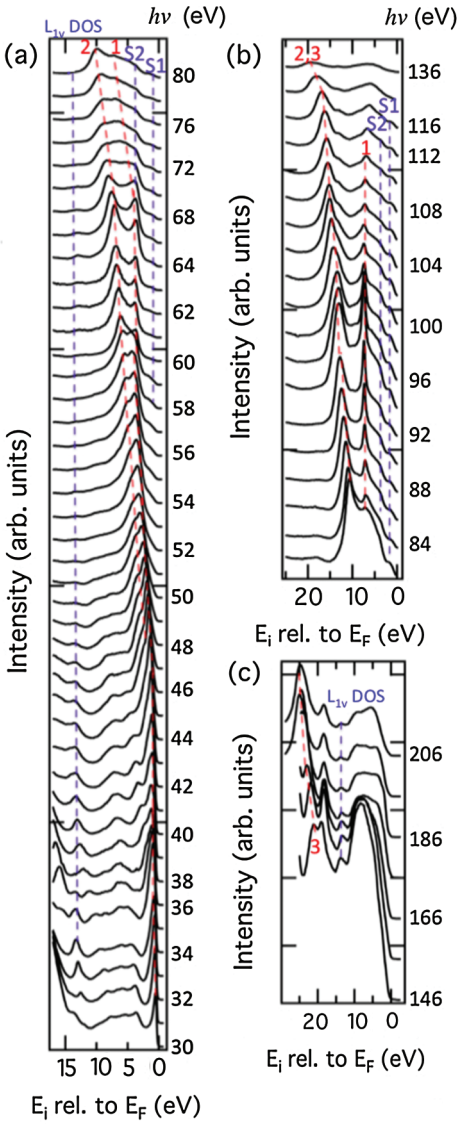

FIG. 1. (Color online) Normal emission angle-resolved energy distribution curves from the C(100):H surface as a function of photon energy $h\nu$ with the initial state energy referenced to the Fermi level. Spectra were taken (a) between $h\nu = 30-80$ eV with a step size of 1 eV between 30–64 eV and 2 eV between 64–80 eV (b) between $h\nu = 82-136$ eV with a step size of 2 eV between 82–112 eV and 10 eV between 116–136 eV, and (c) between $h\nu = 146-206$ eV with a step size of 10 eV.

116–136 eV. (c) $h\nu = 146-206$ eV with a step size of 10 eV. There are two types of features evident in the EDCs: primary photoelectron peaks, which disperse in binding energy with photon energy, and a set of smaller emission peaks, which exhibit a constant binding energy. Since we are performing a normal emission experiment on a three-dimensional material, the assignment of these transitions as from the bulk or surface is straightforward; those peaks, which disperse with photon energy are due to transitions from the bulk band structure, whilst those that are dispersionless are due to surface related bands, which do not exhibit any dispersion at all in $\vec{k}_{\perp i}$ or due to density-of-states effects as will be discussed below.

A. Determining the inner potential V_0

The primary peaks in Fig. 1 originate from the bulk diamond valence band, as these features disperse as expected for direct transitions within the bulk band structure. The turning points (in binding energy) in the E_i versus $h\nu$ sequence of these primary peaks mark direct transitions occurring at the Brillouin zone center and boundary crossings.[35] These can be used to determine an experimental value for the inner potential in Eq. (1) and to check the validity of the nearly-free-electron final-state dispersion. A minimum binding energy (corresponding to a transition from the valence-band maximum) occurs at $E_i = -0.51 \pm 0.035$ eV for $h\nu = 30$ eV, which originates from a transition at the zone center (Γ_{25}^{+v}) with $\vec{k}_{\perp f} = 2(2\pi/a) = 2\Gamma\Delta X$ in the extended-zone scheme, and hence $\vec{k}_{\perp i} = 0$ in the reduced zone scheme. Thus the value of 0.51 eV corresponds to the distance of the Fermi energy to the valence-band maximum (VBM) and all energies given relative to E_F can therefore be corrected by this value to yield their energies relative to VBM. Using Eq. (1), this gives $V_0 = -22.23$ eV. A similar value of $V_0 = -21.88$ eV is calculated from the turning point at the zone boundary (X_{4v}), which occurs at $E_i = E_F - 7.48$ eV for $h\nu = 96$ eV. Our values for V_0 agree reasonably well with the value of -23 eV used by Yokoya *et al.* for [111] diamond.[16] This is to be expected because V_0 as a property of the bulk band structure should not depend on the surface orientation. Having established an average value of -22.06 eV for the inner potential, we are now in a position to determine E_i as a function of $k_\perp$ for the primary peak positions labeled 1–3 in Fig. 1. The results of performing this mapping are shown in Fig. 2 and are discussed in the following sections.

B. Dispersionless features of the (100) surface

In Fig. 1(b), there are two dispersionless features, at $E_F - E_i = 1.70 \pm 0.075$ eV and 3.82 ± 0.075 eV, that arise from emission due to occupied surface states; we refer to these as S1 and S2 in Figs. 1 and 2, respectively. The surface state S1 has previously been studied using photoemission for photon energies between 35 and 50 eV,[18–21] with all references reporting a feature at the Γ point with an energy between 1.3 and 1.9 eV below E_F. Graupner *et al.* show by varying the photon energy from 35 to 50 eV that this feature is a combination of a surface resonance and a direct transition from the bulk valence band of diamond, so that a reliable value for the energy of this surface state has not been obtained.[20]

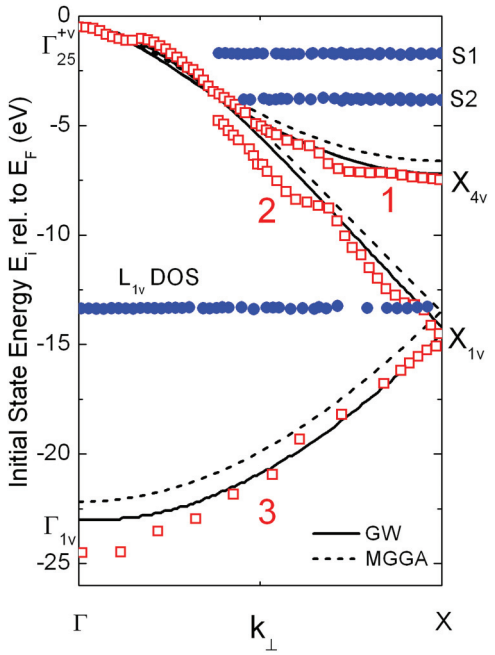

FIG. 2. (Color online) Valence-band dispersions $E(\vec{k})$ of hydrogen-terminated diamond along the Γ-Δ-X direction from normal emission spectra. Red squares represent the band dispersion and circles represent the dispersionless band features, both experimentally obtained. Solid lines represent the GW calculated band structure and the dashed lines represent an MGGA band structure calculated by the authors.

However, by using higher photon energies to separate the different emission processes as it is done here, a true position of 1.7 eV below E_F for this surface state resonance at the Γ point is determined. The position of the second state is consistent with Diederich *et al.* who report on a spectral feature, which is also attributed to a surface state in resonance with a bulk state, at the energy of 3.7 eV below E_F.[21] Both of the surface states S1 and S2 reported here are in agreement with theoretical energies calculated by Furthmüller *et al.*[37]

The dispersionless feature at $E_F - E_i = 13.34 \pm 0.075$ eV is not due to a surface resonance but rather related to non-k-conserving transitions at the energy that corresponds to the high and sharp peak in the DOS that arises from flat portions of the band structure at the L_{1V} critical point in the diamond band structure. Ideally, DOS-related structures should not contribute to an ARPES spectrum of an ideal surface. However, bulk and surface defects act as scattering centers and provide the necessary **k** vector to scatter electrons from the L point into the detection direction. Indeed, the contribution of these states to the EDCs of Fig. 1 is very weak compared to the much larger peak reported by Maier *et al.*[38] for the same transition. This attests to the good surface quality of our sample and supports our assignment of defect scattering rather than intrinsic surface photoemission, which can also give rise to a component resembling the density of states.[39] This same feature has previously been reported by Maier *et al.* at 12.8 ± 0.1 eV below the VBM.[38] Correcting that value with the $E_F - E_{\mathrm{VBM}} = 0.51 \pm 0.035$ eV deduced above for our sample yields 13.3 eV below E_F in perfect agreement with our value.

TABLE I. Critical point energies (in electron volts) at the Γ and X points of diamond.

	Expt. (This work)	MGGA (This work)	GW (This work)	LMTO (LDA) (other authors)	GW (other authors)	Expt. (other authors)
Γ_{1v}	-24.0 ± 0.5	-21.68	-22.0	-21.90[9]	-23.0[11,14]	-21.0 ± 1.0[15]
				-21.35[13]	-23.42[13]	-23.0 ± 0.2[40]
						-24.2 ± 1.0[41]
						-23.5 ± 0.5[17]
Γ'_{25v}	0.0	0.0	0.0	0.0	0.0	0.0
X_{4v}	-6.97 ± 0.075	-6.12	-6.74	-6.66[9]	-6.86[13]	–
				-6.26[13]	-6.71[14]	
X_{1v}	-14.01 ± 0.075	-12.98	-13.42	-13.16[9]	-14.15[13]	–
				-12.61[13]	-13.70[14]	
Γ_c	28.60	27.69	28.10	26.33[9]		15.0[15]
	31.10	29.55	28.50	31.23 [9]		24.0[15]
	38.60	37.47	35.40	32.49[9]		
X_c	23.94	25.85	24.46	24.40 [9]		–
	36.19	34.20	32.77			
	57.19	40.14	39.90			
		51.20	50.60			
		52.75				
		56.60				

C. Critical point energies in the valence-band structure

Moving now to the valence-band dispersions, from Fig. 2 the critical valence-band points Γ_{1v}, X_{4v}, and X_{1v} relative to E_F have been measured at -24.53 ± 0.5 eV ($h\nu = 196$ eV), -7.48 ± 0.075 eV ($h\nu = 94$ eV), and -14.51 ± 0.075 eV ($h\nu = 100$ eV), respectively. Using the value of $E_F - E_{\mathrm{VBM}} = 0.51$ eV determined earlier, we obtain $\Gamma_{1v} = -24.0 \pm 0.5$ eV, $X_{4v} = -6.97 \pm 0.075$ eV, and $X_{1v} = -14.0 \pm 0.075$ eV with respect to the top of the valence band, Γ_{25}^{+v}.

Table I compares our experimentally determined critical point energies and theoretical results (DFT, G_0W_0, and self-consistent GW calculations) with various theoretical and experimental values reported in the literature.[9,11,13–15,17,40,41] From Table I, the experimentally determined energies for both X_{4v} and X_{1v} are much better reproduced by GW than standard DFT calculations. In particular, the agreement with the results of Rohlfing *et al.*[13] is excellent, differing by only ∼0.1 eV, which is within the experimental error. For Γ_{1v} (width of the valence band), the result presented here differs from the experimental ARPES work of Yokoya *et al.* by 0.5 eV[17] and that of Jiménez *et al.* on [111] diamond by 1.0 eV.[40] However, at the high photon energies required to probe the bottom of the valence band, transitions into final-state bands are significantly broadened, so agreement to within 1.0 eV is not unreasonable. Interestingly, our result is in excellent agreement with that of McFeely *et al.*[41] who derived the valence-band width not by ARPES but from a measurement of the width of the total density of states using a fixed, high-energy photon source (Al $K_\alpha = 1486.6$ eV). The close agreement between the experimentally determined critical point energies and first-principles quasiparticle calculations, as opposed to DFT, shows that many-body effects such as dynamic screening are important even for wide-band gap semiconductors such as diamond, as detailed by Jiménez *et al.*[40]

D. Critical point energies in the conduction band

From the critical valence-band points at Γ_{25}^{+v} and X_{4v}, constant initial state spectroscopy (CIS) was performed for photoelectrons emitted normal to the hydrogen-terminated diamond (100) surface. Here, the transition intensity from a fixed initial state energy is monitored as a function of photon energy, in order to probe the location of unoccupied band states.[15] Figure 3 plots the transition intensity as a function of photon energy from (a) the top of the valence band ($\Gamma_{25}^{+v} = E_v$) and (b) the X point corresponding to X_{4v}. Peaks in these graphs correspond to transitions from the occupied critical points to unoccupied final-state bands, with the absolute photon energy yielding the energy difference and thus the unoccupied band position relative to the critical point. Comparing the peak energies in the spectra to theoretically predicted values in Table I (with all energies referenced to Γ_{25}^{+v}), we observe a good overall agreement with our theoretically determined values. The peaks at higher photon energy are asymmetric and significantly broadened, suggesting the presence of multiple unoccupied bands that are unresolved, rather than a single band. This is indeed confirmed by the theoretical calculations shown in Table I and also in Fig. 3(c), which shows the calculated MGGA and GW conduction bands relative to Γ_{25}^{+v}. The large broadening may also be due to energy-dependent lifetime effects and matrix elements involving many-body effects. By mapping the unoccupied bands of diamond that lie well above the conduction-band minimum, we have shown that the agreement between experiment and theory is actually quite good, particularly for the MGGA band structure where only a simple "scissors" correction was used to correct for the underestimation of the band gap.

E. Modulations in the experimental valence-band dispersion

As shown earlier, the agreement between the experimentally determined occupied band energies and GW calculations

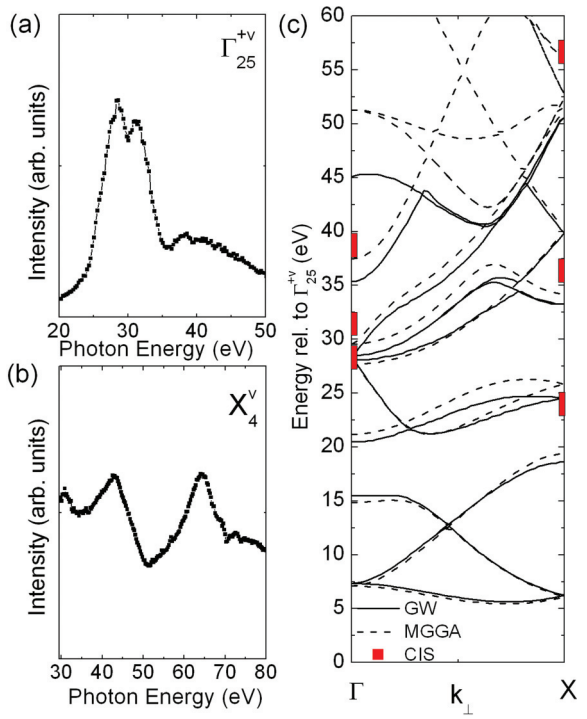

FIG. 3. (Color online) Constant initial state spectra (CIS) for photoelectrons emitted normal to the hydrogen-terminated diamond (100) surface for an initial state energy fixed at: (a) Γ_{25}^{+v} and (b) X_{4v}, with the photon energy stepped by 0.25 eV to map transitions into unoccupied final-state bands. (c) Calculated band structure of the conduction band where the solid lines represent the GW band structure, dashed lines represent the MGGA band structure, and the red squares represent the extracted CIS critical point energies.

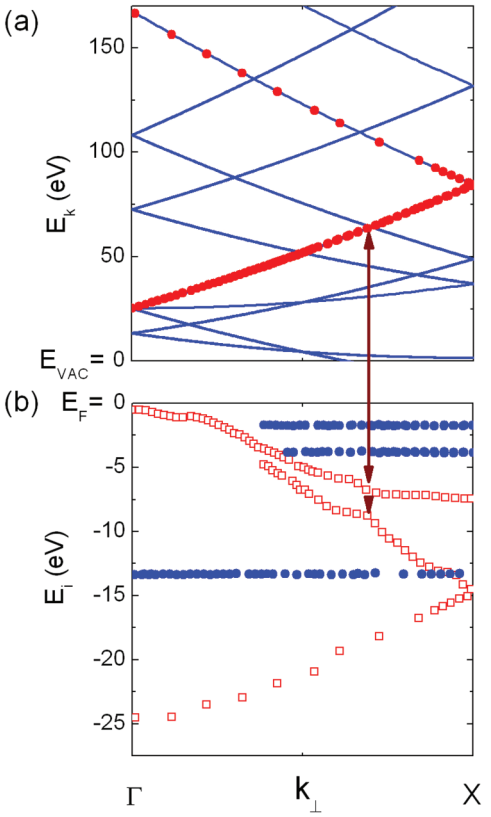

FIG. 4. (Color online) (a) Red circles represent the measured photoelectron kinetic energy of the peaks identified in Fig. 1 as a function of $k_\perp$ determined from Eq. (1) using $V_0 = -22.06$ eV, and free-electron bands along Γ-X calculated for a diamond lattice (blue lines) relative to the vacuum level. (b) Measured initial state energy E_i as a function of $k_\perp$ (data from Fig. 2). Red squares represent the valence-band dispersions and the blue circles represent surface related features. The maroon arrow indicates the primary cone band crossing with the G_{11} secondary band in the zone folded FEFS model lined against the "kinks" in the measured occupied band structure.

is excellent at the critical points. However, in Fig. 2 away from the Γ and X, there appear to be kinks in the valence-band dispersion that are at odds with the smooth band dispersion predicted theoretically. These kinks can have two reasons: uncertainty in the assigned binding energy or uncertainty in the mapped $k_\perp$. The former case holds for the kink at around ∼1.5 eV below the Fermi level and at $k_\perp \sim 0.2$ Γ-X. Here, the kink arises from the overlap of the bulk valence band with emission with that from the surface resonance S1 such that it is difficult to resolve the two independent structures accurately in binding energy, as it was also seen by Graupner *et al.* in their study.[20] The kink at the energy of ∼3.5 eV below the Fermi level can be attributed to the same issue, as here the bulk transitions closely approach the S2 surface resonance, and again, it is difficult to resolve the direct transition's energetic position.

However, the modulations occurring in the energy range between 5 and 10 eV below the Fermi level and at $k_\perp \sim 0.7$ Γ-X cannot be explained in a similar fashion. In Fig. 4, we show that these modulations occur at $k_\perp$ points, where the primary final-state free-electron parabola is crossed by other free-electron bands not belonging to the primary cone emission. For the intersection at $k_\perp \sim 0.7$ Γ-X, this corresponds to the $G_{11} = 2\pi/a(-3, -1, -1)$ free-electron band. A single primary cone FEFS is clearly an oversimplification at these crossing points where perturbation of the band dispersion is known to occur that lifts the degeneracy.[42] In order to determine the perturbation in the final state, the initial state energies are placed at $k_\perp$ points where they follow the expected smooth band dispersion [see Fig. 5(a)]. The corresponding final-state energies are plotted in Fig. 5(b) as points and squares superimposed on the free-electron final states. It is evident that right at the crossing, a gap of about 3.7 eV opens up that corresponds to $2V(G_{311})$, where $V(G_{311}) = 1.85$ eV is the pseudopotential form factor that mixes the two free-electron bands, in good agreement with the pseudopotential form factor calculated by Saslow *et al.* of 1.8 eV.[43] While the final-state bands labeled 1 and 2 follow the disturbed band structure close to the former crossing point, it is also evident that there are substantial deviations from the final states adjacent to the former crossing. It appears that the initial states of band 2 try to follow the secondary band for about 10% of the BZ dimension below the crossing point before they join the primary cone again whereas band 1 does the same above the crossing point. It appears that this behavior is due to the competing requirements of symmetry-dictated matrix elements and geometrically favored primary cone emission. Alternatively, the observed peak in the spectrum is a superposition of two transitions with varying intensity

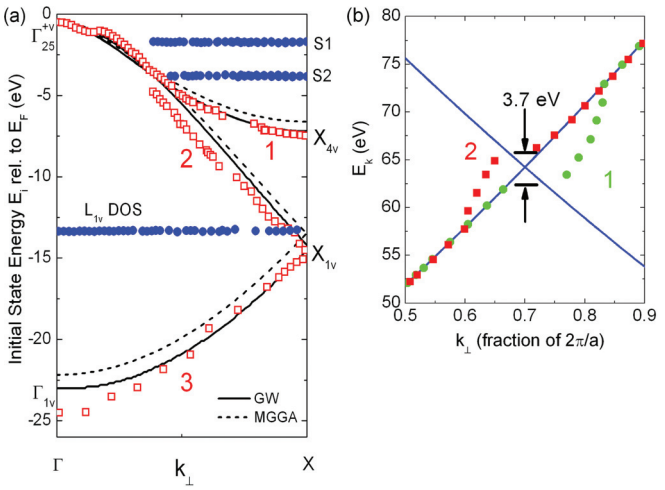

FIG. 5. (Color online) (a) Corrected valence-band dispersion of hydrogen-terminated diamond same as Fig. 2 except the initial state energies have been placed at $k_\perp$ points where they follow the expected band dispersion to account for the failure of the FEFS model at the final-state band crossing point. (b) Measured photoelectron kinetic energy as a function of corrected $k_\perp$. Blue lines represent the calculated free-electron bands, corrected final-state dispersion of band 2 (red squares) and band 1 (green circles).

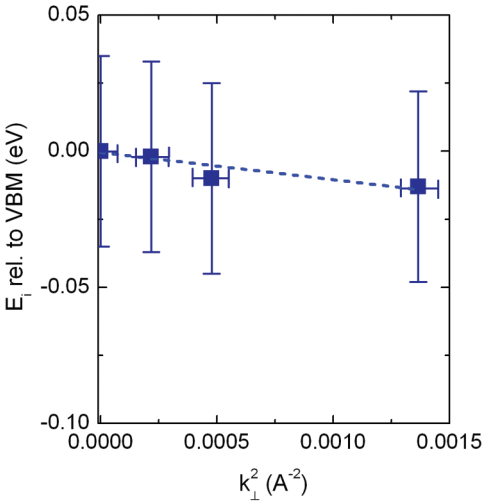

FIG. 6. (Color online) Initial state energy E_i relative to VBM vs k^2 close to the Γ point. Dashed line is a linear fit of the data, yielding an effective mass of $(0.39 \pm 0.30)m_0$.

that correspond to the "main" transition and the transition to the split-off band with decreasing intensity as one moves away from the former crossing point. This would result in the observed dispersion of the mean position. However, aside from these band crossing points, it is clear that the FEFS model is remarkably successful in mapping the band dispersion of diamond along [100] in normal emission.

F. One band effective mass [100] at Γ

The hole effective masses of diamond for the light hole, heavy hole, and split-off band can, in principle, be determined from the valence-band dispersion near the Γ point. Using the $\mathbf{k} \cdot \mathbf{p}$ perturbation theory, Willatzen *et al.* [9] calculated the light hole, heavy hole, and split-off band masses along [100] to be $m_{\rm lh} = 0.366\ m_0$, $m_{\rm hh} = 0.427\ m_0$, and $m_{\rm so} = 0.394\ m_0$, which gives an average one-band effective mass of $0.396\ m_0$.[44] Due to its small spin-orbit splitting of only 13 meV,[10] it is not possible to resolve the light hole, heavy hole, and split-off band of diamond near the Γ point in an ARPES experiment. Instead, only a single band is resolved as shown in Fig. 2 from which we can estimate the one-band effective mass. In order to obtain sufficient data in the immediate vicinity around the Γ point (corresponding to $h\nu = 30$ eV), a series of normal emission EDCs with photon energy stepped in 0.2 eV increments were taken to obtain a plot of E_i as a function of $k_\perp^2$ around Γ as shown in Fig. 6. The slope in the linear region yields the one band average effective mass along [100] of $m_{\rm aver} = (0.39 \pm 0.30)m_0$ in very good agreement with the theoretically derived value. The error accounts for the experimental energy resolution of 70 meV at $h\nu = 30$ eV determined from the width of Fermi edge of the Au reference. There are, in principle, further limitations to this approach related to the intrinsic accuracy of three-dimensional band mapping.[45] The intrinsic initial state energy broadening characterized by the hole lifetime, $\delta E = \hbar/\tau_h$, amounts to an energy broadening of $\sim$10 μeV, which is negligible given the recombination carrier lifetimes in diamond are typically $\sim$1 ns.[46] The uncertainty in $k_\perp$ is given by $\delta k_\perp = \lambda^{-1}$. For an inelastic mean free path $\lambda = 10$ Å, (at an electron kinetic energy of 25 eV) this amounts to about 5% of the Brillouin zone dimension along Γ-Δ-X. This uncertainty requires that we put our result in perspective against other means of determining the carrier effective mass. Diamond effective masses have been experimentally determined through cyclotron resonance measurements by Rauch *et al.*[47] (giving $m_{\rm lh} = 0.72\ m_0$, $m_{\rm hh} = 2.0\ m_0$, and $m_{\rm so} = 1.06\ m_0$) and Kono *et al.*[22] ($m_{\rm lh} = 0.55\ m_0$, $m_{\rm hh} = -2.13\ m_0$, and $m_{\rm so} = 1.49\ m_0$), illustrating the significant uncertainty in our present knowledge of the hole effective masses in diamond. Hence the value of $0.39 \pm 0.30\,m_0$ determined here for the average one-band effective mass gives considerable confidence in the effective hole masses as calculated in Ref. 9 in contrast to one-band masses of $1.26\,m_0$[47] and $-0.03m_0$[22] derived from cyclotron resonance measurements.

IV. CONCLUSION

In summary, we have presented a detailed evaluation of the valence-band dispersion of diamond along [100] using normal emission ARPES interpreted within a FEFS framework. An excellent agreement has been found with GW calculations, particularly, at the critical point energies. Deviations between experiment and theory in the valence-band dispersion are shown to correspond to the lifting of band crossings of the free-electron final states, such that the FEFS is clearly an oversimplification of the final-state band structure at these points. A one-band effective mass of $0.39\,m_0$ is determined from the band dispersion close to the Γ point, which puts to rest some of the contradictions over experimental results in the literature.

ACKNOWLEDGMENTS

We acknowledge financial support from the Australian Research Council under DP0879827 and the Australian Synchrotron International Synchrotron Access Program (ISAP). This work was supported by the Multi-modal Australian Sciences Imaging and Visualisation Environment (MASSIVE) (www.massive.org.au). ARPES measurements were performed at beamlines U112 and U49 BESSY II Synchrotron, Berlin, Germany. The authors would like to acknowledge M. Cardona for fruitful discussions related to the carrier effective masses.

*mtedmonds@students.latrobe.edu.au

[1] H. Kawarada, M. Aoki, and M. Ito, Appl. Phys. Lett. **65**, 1563 (1994).

[2] K. Ueda, M. Kasu, Y. Yamauchi, T. Makimoto, M. Schwitters, D. J. Twitchen, G. A. Scarsbrook, and S. E. Coe, IEEE Electron Devices **27**, 570 (2006).

[3] H. Kawarada, Y. Araki, T. Sakai, and T. Ogawa, Phys. Status. Solidi A **185**, 79 (2001).

[4] J. A. Garrido, A. Härtl, S. Kuch, M. Stutzmann, O. Williams, and R. Jackman, Appl. Phys. Lett. **86**, 073504 (2005).

[5] J. Ristein, W. Zhang, and L. Ley, Phys. Rev. E **78**, 041602 (2008).

[6] C. E. Nebel, B. Rezek, D. Shin, H. Uetsuka, and N. Yang, J. Phys. D: Appl. Phys. **40**, 6443 (2007).

[7] J. B. Cui, J. Ristein, and L. Ley, Phys. Rev. Lett. **81**, 429 (1998).

[8] M. V. G. Dutt, L. Childress, L. Jiang, E. Togan, J. Maze, F. Jelezko, A. S. Zibrov, P. R. Hemmer, and M. D. Lukin, Science **316**, 1312 (2007).

[9] M. Willatzen, M. Cardona, and N. E. Christensen, Phys. Rev. B **50**, 18054 (1994).

[10] J. Serrano, M. Cardona, and T. Ruf, Solid State Commun. **113**, 411 (2000).

[11] M. S. Hybertsen and S. G. Louie, Phys. Rev. B **34**, 5390 (1986).

[12] R. W. Godby, M. Schlüter, and L. J. Sham, Phys. Rev. B **37**, 10159 (1988).

[13] M. Rohlfing, P. Krüger, and J. Pollmann, Phys. Rev. B **48**, 17791 (1993).

[14] H. Löfås, A. Grigoriev, J. Isberg, and R. Ahuja, AIP Advances **1**, 032139 (2011).

[15] F. J. Himpsel, J. F. van der Veen, and D. E. Eastman, Phys. Rev. B **22**, 1967 (1980).

[16] T. Yokoya, T. Nakamura, T. Matsushita, T. Muro, Y. Takano, M. Nagao, T. Takenouchi, H. Kawarada, and T. Oguchi, Nature (London) **438**, 647 (2005).

[17] T. Yokoya, T. Nakamura, T. Matsushita, T. Muro, H. Okazaki, M. Arita, K. Shimada, H. Namatame, M. Taniguchi, Y. Takano, M. Nagao, T. Takenouchi, H. Kawarada, and T. Oguchi, Sci. Technol. Adv. Mater. **7**, S12 (2006).

[18] J. Wu, R. Cao, X. Yang, P. Pianetta, and I. Lindau, J. Vac. Sci. Technol. A **11**, 1048 (1993).

[19] G. Francz, P. Kania, G. Gantner, H. Stupp, and P. Oelhafen, Phys. Status Solidi **154**, 91 (1996).

[20] R. Graupner, M. Hollering, A. Ziegler, J. Ristein, L. Ley, and A. Stampfl, Phys. Rev. B **55**, 10841 (1997).

[21] L. Diederich, P. Aebi, O. M. Küttel, E.-M. Schaller, R. Fasel, and L. Schlapbach, Surf. Sci. **393**, L77 (1997).

[22] J. Kono, S. Takeyama, T. Takamasu, N. Miura, N. Fujimori, Y. Nishibayashi, T. Nakajima, and K. Tsuji, Phys. Rev. B **48**, 10917 (1993).

[23] C. L. Lee, E. Gu, M. D. Dawson, I. Friel, and G. Scarsbrook, Diam. Relat. Mater. **17**, 1292 (2008).

[24] L. Ley, Diam. Relat. Mater. **20**, 418 (2011).

[25] As quoted by supplier Element6; www.e6cvd.com

[26] M. Riedel, J. Ristein, and L. Ley, Phys. Rev. B **69**, 125338 (2004).

[27] L. Broekman, A. Tadich, E. Huwald, J. D. Riley, R. C. G. Leckey, T. Seyller, K. V. Emstev, and L. Ley, J. Electron Spectrosc. Relat. Phenom. **144**, 1001 (2005).

[28] http://elk.sourceforge.net/

[29] F. Tran and P. Blaha, Phys. Rev. Lett. **102**, 226401 (2009).

[30] X. Gonze, J.-M. Beuken, R. Caracas, F. Detraux, M. Fuchs, G.-M. Rignanese, L. Sindic, M. Verstraete, G. Zerah, F. Jollet, M. Torrent, A. Roy, M. Mikami, Ph. Ghosez, J.-Y. Raty, and D. C. Allan, Comput. Mater. Sci. **25**, 478 (2002).

[31] S. Lebegue, B. Arnaud, M. Alouani, and P. E. Bloechl, Phys. Rev. B **67**, 155208 (2003).

[32] J. P. Perdew, K. Burke, and M. Ernzerhof, Phys. Rev. Lett. **77**, 3865 (1996).

[33] X. H. Chen, W. Ranke, and E. Schröder-Bergen, Phys. Rev. B **42**, 7429 (1990).

[34] L. S. O. Johansson, P. E. S. Persson, U. O. Karlsson, and R. I. G. Uhrberg, Phys. Rev. B **42**, 8991 (1990).

[35] T.-C. Chiang, J. A. Knapp, M. Aono, and D. E. Eastman, Phys. Rev. B **21**, 3513 (1980).

[36] A. L. Wachs, T. Miller, T. C. Hsieh, A. P. Shapiro, and T.-C. Chiang, Phys. Rev. B **32**, 2326 (1985).

[37] J. Furthmüller, J. Hafner, and G. Kresse, Phys. Rev. B **53**, 7334 (1996).

[38] F. Maier, J. Ristein, and L. Ley, Phys. Rev. B **64**, 165411 (2001).

[39] N. J. Speer, M. K. Brinkley, Y. Liu, C. M. Wei, T. Miller, and T.-C. Chiang, Eur. Phys. Lett. **88**, 67004 (2009).

[40] I. Jiménez, L. J. Terminello, D. G. J. Sutherland, J. A. Carlisle, E. L. Shirley, and F. J. Himpsel, Phys. Rev. B **56**, 7215 (1997).

[41] F. R. McFeely, S. P. Kowalczyk, L. Ley, R. G. Cavell, R. A. Pollak, and D. A. Shirley, Phys. Rev. B **9**, 5268 (1974).

[42] F. Herman, Rev. Mod. Phys. **30**, 102 (1958).

[43] W. Saslow, T. K. Bergstresser, and M. L. Cohen, Phys. Rev. Lett. **16**, 354 (1966).

[44] M. T. Edmonds, C. I. Pakes, and L. Ley, Phys. Rev. B **81**, 085314 (2010).

[45] V. N. Strocov, J. Electron Spectrosc. Relat. Phenom. **130**, 65 (2003).

[46] S. V. Garnov, A. I. Ritus, S. M. Klimentov, S. M. Pimenov, V. I. Konov, S. Gloor, W. Lüthy, and H. P. Weber, Appl. Phys. Lett. **74**, 1731 (1999).

[47] C. J. Rauch, in *Proceedings of the International Conference on the Physics of Semiconductors, Exeter*, edited by A. C. Stickland (Institute of Physics and the Physical Society, London, 1962), p. 276.